


# DNA calorimetric force spectroscopy at single base pair resolution

Received: 6 June 2024

Accepted: 19 February 2025

Published online: 19 March 2025

P. Rissone<sup>1,2</sup>, M. Rico-Pasto<sup>3,4</sup>, S. B. Smith<sup>5</sup> & F. Ritort<sup>1,6,7</sup> 

DNA hybridization is a fundamental molecular reaction with wide-ranging applications in biotechnology. The knowledge of the temperature dependence of the thermodynamic parameters of duplex formation is crucial for quantitative predictions throughout the DNA stability range. It is commonly assumed that enthalpies and entropies are temperature independent, and heat capacity changes  $\Delta C_p$  equal zero. However, it has been known that this assumption is a poor approximation for a long time. Here, we combine single-DNA mechanical unzipping experiments using a temperature jump optical trap with a tailored statistical analysis to derive the ten heat-capacity change parameters of the nearest-neighbor model. Calorimetric force spectroscopy establishes a groundbreaking approach to studying nucleic acids that can be further extended to chemically modified DNA, RNA, and DNA/RNA hybrid structures.

Nucleic acid (NA) thermodynamics is essential to understand duplex formation, where two single strands of DNA or RNA hybridize to form a double helix. Hybridization is a crucial process for genome maintenance with many biotechnological applications, from PCR amplification to gene editing<sup>1–3</sup> and DNA origami<sup>4–6</sup>. Accurate knowledge of the thermodynamic energy parameters of NA hybridization is necessary for developing better protocols, often involving heating and cooling cycles for dissociating and hybridizing complementary strands. Most hybridization studies involve calorimetric melting experiments in bulk, where signals such as heat, UV light absorbance, and fluorescence are measured over samples typically containing  $10^{10}$  molecules in aqueous solutions<sup>7,8</sup>.

Despite recent progress, basic questions about NA hybridization remain unanswered, such as the nature of the transition state and duplex stability far from standard conditions. Examples are extreme cold and high temperatures, molecular condensates, and confined spaces. Thermodynamic predictions far from standard conditions require far-fetched extrapolations of the currently known energy parameters. The heat-capacity change at constant pressure,  $\Delta C_p$ , is crucial for NA formation.  $\Delta C_p$  quantifies the temperature dependence of enthalpy ( $\Delta H$ ) and entropy ( $\Delta S$ ) contributions to the free energy of hybridization through the thermodynamic relations at

constant pressure,  $\Delta C_p = \partial \Delta H / \partial T = T \partial \Delta S / \partial T$ . From a microscopic viewpoint,  $\Delta C_p$  relates to the change in the number of degrees of freedom,  $\Delta n$ , in hybridization reactions according to the equipartition law,  $\Delta C_p = k_B \Delta n / 2$ , with  $\Delta n = 1$  per  $\text{cal mol}^{-1} \text{K}^{-1}$  unit of  $\Delta C_p$ . It has been suggested that the most significant contribution to  $\Delta C_p$  in duplex formation occurs in the alignment of the complementary single-strands upon hybridization<sup>9</sup>.

The temperature dependence of the enthalpy and entropy of DNA hybridization has been neglected for a long time. The assumption  $\Delta C_p = 0$  was mainly adopted as the first scanning calorimetry studies could not detect  $\Delta C_p$ <sup>10</sup>. Over time, improvements in calorimetric measurements<sup>11</sup> pointed out the significant role  $\Delta C_p$  played in DNA hybridization. During the last decades, bulk<sup>12–18</sup> and single-molecule<sup>19–21</sup> experiments assessed the effects of temperature, yielding  $\Delta C_p$  values per bp spanning two orders of magnitude depending on the experimental condition, the technique used and the DNA sequence. Single-molecule methods such as atomic force microscopy<sup>22,23</sup>, FRET<sup>24</sup>, and optical tweezers<sup>25,26</sup> have now reached the maturity to address such challenges. While force spectroscopy derives free energy differences ( $\Delta G$ ) from work measurements, single-molecule FRET does it from the lifetimes of states using the Boltzmann-Gibbs distribution<sup>27</sup>. The mechanical unzipping of single NA hairpins permits measuring the

<sup>1</sup>Small Biosystems Lab, Condensed Matter Physics Departament, Universitat de Barcelona, Barcelona, Spain. <sup>2</sup>Physics Departament, Sapienza University of Rome, Rome, Italy. <sup>3</sup>Unit of Biophysics and Bioengineering, Department of Biomedicine, School of Medicine and Health Sciences, Universitat de Barcelona, Barcelona, Spain. <sup>4</sup>Institute for Bioengineering of Catalonia (IBEC), The Barcelona Institute for Science and Technology (BIST), Barcelona, Spain. <sup>5</sup>Steven B. Smith Engineering, Los Lunas, NM, USA. <sup>6</sup>Reial Acadèmia de Ciències i Arts de Barcelona (RACAB), Secció Física.2a, Barcelona, Spain. <sup>7</sup>Institut de Nanociència i Nanotecnologia (IN2UB), Barcelona, Spain. ✉ e-mail: [ritort@ub.edu](mailto:ritort@ub.edu)

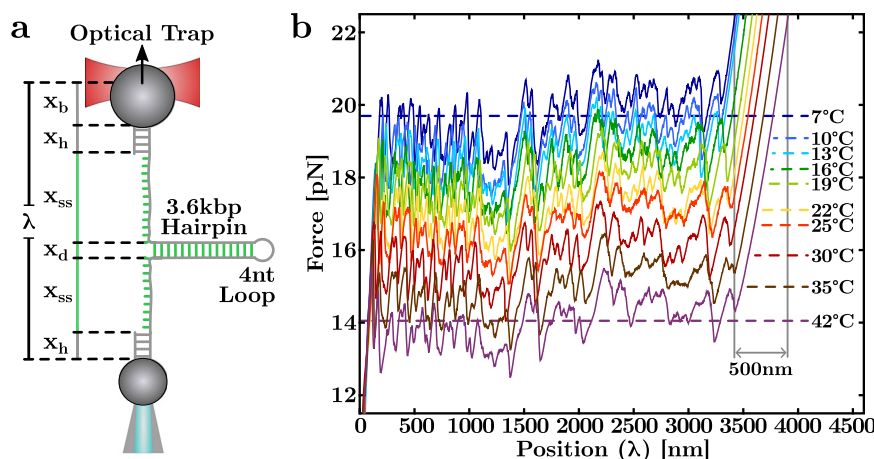


**Fig. 1 | Single-molecule calorimetric force-spectroscopy.** **a** Experimental setup (Sec. 1, “Methods”) showing each component of the (measured) total trap-pipette distance,  $\lambda$ . The hairpin is made of a 3.6 kbp stem ending in a 4 nucleotide (nt) loop. **b** Temperature dependence of FDCs obtained by pulling the 3.6 kbp DNA hairpin.

At each  $T$ , the FDC results from averaging over 5–6 molecules for 40–50 unzipping/rezipping cycles (see also Supplementary Figs. 1 and 2). Source data are provided as a Source Data file.

folding free energy landscape along the reaction coordinate defined by the number of released nucleotides during the unzipping process<sup>28,29</sup>. The unzipping reaction finds applications in the footprinting of DNA-binding restriction enzymes<sup>30</sup>, transcription factors<sup>31,32</sup>, and peptides<sup>33</sup>. Mechanical unzipping has also permitted the design of calipers for measuring molecular distances<sup>34</sup>. Here, we derive the elusive heat capacity change  $\Delta C_p$  for the different DNA nearest-neighbor base pair motifs.

DNA’s thermodynamic stability ( $\Delta G$ ) results from the compensation of the favorable  $\Delta H$  and the unfavorable  $\Delta S$  of folding,  $\Delta G = \Delta H - T\Delta S$ , with  $T$  the temperature. For  $\Delta C_p = 0$ ,  $\Delta H$  and  $\Delta S$  are  $T$ -independent, and  $\Delta G$  is linear with  $T$ . For  $\Delta C_p \neq 0$ , enthalpy-entropy compensation makes  $\Delta H$  and  $T\Delta S$  of comparable magnitude masking deviations of  $\Delta G$  from a  $T$ -linear behavior. Potentially, one could derive the temperature-dependent  $\Delta S$  from  $\Delta G$  using the relation  $\Delta S = -\partial\Delta G/\partial T$ . However, this method is imprecise due to strong compensation between  $\Delta H$  and  $T\Delta S$ . To determine  $\Delta C_p$ , it is convenient to measure either enthalpy or entropy contributions independently of  $\Delta G$ . We introduce a method to accurately derive DNA thermodynamics by directly measuring the temperature-dependent entropy of hybridization  $\Delta S$  using calorimetric force spectroscopy with optical tweezers<sup>20</sup>. We apply the Clausius-Clapeyron equation to single-molecule experiments<sup>35</sup> and combine it with a tailored machine-learning algorithm. This approach allows us to derive the entropies, enthalpies, and  $\Delta C_p$  parameters of hybridization at single base pair resolution in the nearest-neighbor (NN) model<sup>36,37</sup>.

According to the NN model, the duplex’s free energy, entropy, and enthalpy equal the sum of all contributions of the adjacent nearest-neighbor base pairs (NNBP) along the sequence. The four distinct canonical Watson-Crick base pairs generate sixteen possible NNBP combinations (e.g., AG/TC, meaning that 5′–AG–3′ hybridizes with 3′–TC–5′) with their corresponding energy parameters. The sixteen parameters reduce to ten due to strand complementarity symmetry (e.g., AG/TC equals CT/GA), further reducing to eight from circular symmetry relations<sup>38–40</sup>. The ten NNBP DNA parameters have been derived at 37 °C from melting experiments of short DNA duplexes by many laboratories worldwide<sup>41–45</sup> and unified by Santalucia et al.<sup>46</sup> in the so-called Unified Oligonucleotide (UO) set. In the last decade, the NNBP free energy parameters have been derived from reversible work measurements in mechanical unzipping experiments of DNA and RNA hairpins at room temperature (298K)<sup>29,40,47</sup>. These energy parameters are used by most secondary structure prediction tools, such as Mfold<sup>48</sup>, Vienna package<sup>49</sup>, uMelt<sup>50</sup>, among others. Here,

we apply calorimetric force spectroscopy to measure the NNBP energy parameters in the temperature range 7–40 °C and derive the  $\Delta C_p$  values.

## Results

We used a temperature-jump optical trap (Fig. 1a and Sec. 1, Methods) to unzip a 3593bp ( $\approx 3.6$  kbp) DNA hairpin ending in a GAAA tetraloop. Pulling experiments were conducted at temperatures 7–42 °C at 1M NaCl in 10 mM Tris-HCl buffer (pH 7.5). In Fig. 1b and Supplementary Figs. 1, 2, we show the measured force-distance curves (FDCs). They exhibit a sawtooth pattern upon increasing the trap-pipette distance,  $\lambda$ , until the hairpin unzips completely and the elastic response of the released single-stranded DNA (ssDNA) is measured (rightmost part of Fig. 2b). Upon increasing  $T$ , the hairpin unzips at progressively lower forces (horizontal dashed lines in Fig. 1b) from  $\sim 20$  pN at 7 °C to  $\sim 14$  pN at 42 °C. This indicates that the DNA stability decreases with  $T$ , and the energy parameters of the NN model are temperature dependent: the higher the temperature, the lower the hairpin’s free energy of hybridization. Moreover, the molecular extension of the ssDNA at a given force increases with  $T$ , yielding a total of  $\sim +500$  nm between 7° and 42 °C (Fig. 1b, horizontal grey double arrow).

### T-dependence of the ssDNA elasticity

Deriving the full NNBP parameters in unzipping experiments requires measuring the  $T$ -dependent ssDNA elasticity. To do this, we extracted the force versus the hairpin’s molecular extension ( $x$ ) curve (hereafter referred to as FEC) by using the relation

$$\lambda = x + x_b + 2x_h \Rightarrow x = \lambda - x_b - 2x_h, \quad (1)$$

with  $x$  being shown as a green vertical line in Fig. 1a. Here,  $x_b$  and  $2x_h$  are the bead displacement relative to the trap’s center and the handles extension, respectively (grey vertical lines in Fig. 1a). Notice that all extensions are  $f$  and  $T$  dependent. To determine the term  $x_b + 2x_h$  in Eq. (1), we have used the effective stiffness method<sup>51</sup> with  $x_b + 2x_h = f/k_{\text{eff}}$  and  $x = \lambda - f/k_{\text{eff}}$  (Supplementary Methods, Sec. 2) where  $k_{\text{eff}}$  is obtained from a linear fit to the first FDC slope, i.e., when the hairpin is fully folded (Supplementary Figs. 3 and 4). This gives the FEC at each  $T$  (Supplementary Fig. 5).

From Fig. 1a,  $x = x_{\text{ss}} + x_d$ , where  $x_{\text{ss}}$  is the ssDNA extension and  $x_d$  is the projection of the helix diameter ( $d = 2$  nm<sup>52</sup>) on the pulling axis, which is described by Eq. (7) (Methods). To model the ssDNA elasticity, we used the inextensible WLC model<sup>53,54</sup> (Sec. 2, Methods). In this

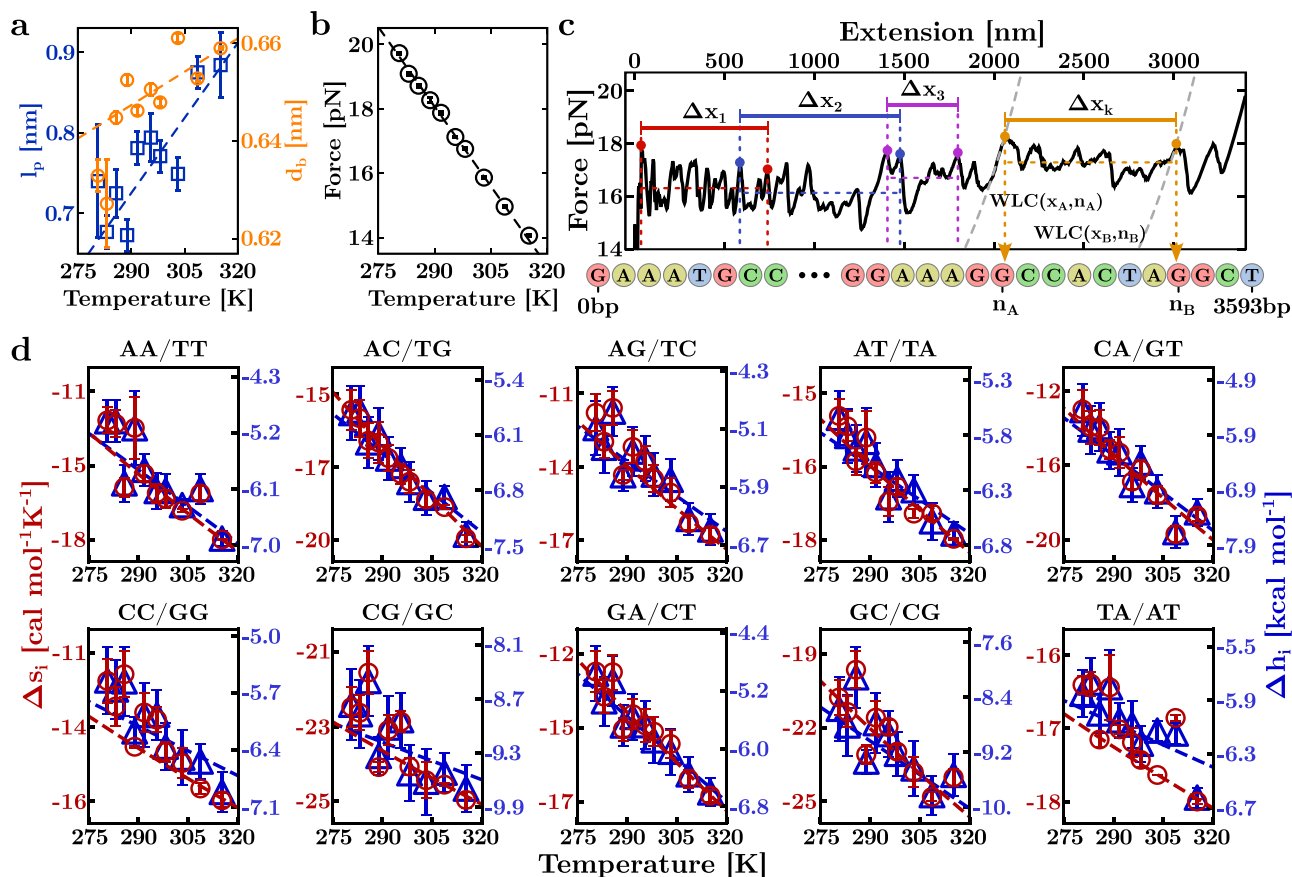


**Fig. 2 | NNBP entropies and enthalpies.** **a, b**  $T$ -dependence of the persistence length,  $l_p$ , (blue) interphosphate distance,  $d_b$ , (orange) and average unzipping force,  $f_m$  (black). Linear fits to data (black, blue, and orange lines, respectively) are also shown. **c** Example of application of the Clausius-Clapeyron relation to the experimental FEC (see text). **d**  $T$ -dependence of the ten NNBP entropies (red) and

enthalpies (blue). Results are reported in Supplementary Tables 4 and 6, respectively. The entropy of motifs GC/CG and TA/AT were obtained by applying the circular symmetry relations. Fits to data (see text) are shown with a red (entropy) and blue (enthalpy) dashed line. All data are presented as mean values  $\pm$  SE (see also Supplementary Methods, Sec. 5). Source data are provided as a Source Data file.

model, the extension  $x_{ss}$  at a given force is proportional to the number of released bases  $n$ ,  $x_{ss}(f, T) = nx_{ss}^{(1)}(f, T)$  where  $x_{ss}^{(1)}$  is the extension per base. For the fully folded hairpin,  $n = 0$  and  $x = x_d$ , whereas for the fully unzipped hairpin,  $x = 2x_{ss} = 2(N + L/2)x_{ss}^{(1)}$  with  $N$  the number of base pairs in the stem and  $L$  the loop size. At a given  $T$ , we measured  $x_{ss}^{(1)}(f, T)$  by fitting the WLC in Eq. (6) (Methods) to the FEC after the last force rip, i.e., where the hairpin is fully unfolded and  $n = 2(N + L/2)$  (Supplementary Fig. 3). Applying this procedure to the FECs at all  $T$ , gives the temperature-dependent persistence length ( $l_p$ ) and interphosphate distance ( $d_b$ ) of the ssDNA (Fig. 2a and Supplementary Table 3). As  $T$  increases,  $l_p$  (blue squares), varies from  $l_p^{280K} = 0.74(7)$  nm to  $l_p^{315K} = 0.88(4)$  nm ( $\approx +30\%$ ). A linear fit to the data gives the slope  $6(1) \cdot 10^{-3}$  nm/K (blue line). Moreover, the interphosphate distance,  $d_b$ , (orange circles) shows a weak linear  $T$ -dependence ( $\approx +5\%$ ) of slope  $4(1) \cdot 10^{-4}$  nm/K (orange line). Similar behavior has been observed for shorter ssDNAs of 20–40 nucleotides<sup>55</sup> and polypeptide chains<sup>35</sup>. The observed increase in  $x_{ss}$  with  $T$  is predicted in Debye-Huckel theory due to the entropy of the cloud of counterions. Upon increasing temperature, the screening of the phosphates repulsion is reduced, and  $l_p$  increases. Our results confirm this trend with  $l_p$  increasing with temperature tenfold relative to  $d_b$ , which remains almost constant in the studied temperature range.

### Derivation of the NNBP entropies

To derive the entropies of the different NNBP, we have decomposed the full unzipping curve into segments of variable length encompassing different regions along the FEC. Each segment is delimited by two

peaks corresponding to force rips along the FEC. The peaks have been selected by looking for local maxima along the experimental signal. To do so, the FEC function derivatives have been numerically computed, and the maxima were determined by imposing  $df(x)/dx = 0$ . We notice that the magnitude of the force rip is proportional to the number of released bases in that unfolding event. To ensure the maximal signal-to-noise ratio, we discarded events within the FEC statistical errors by only accounting for force-rips with  $\Delta f \geq 2$  pN. Figure 2c shows examples of segments starting and ending at a peak (colored circles). Considering all possible combinations of starting and ending peaks, a set of  $K$  segments has been obtained for each  $T$ . Note that peaks are not necessarily consecutive, as different segments can overlap, making the analysis more robust. In a single unzipping curve, the typical number of peaks is  $N_p \sim 30 - 35$  (see Fig. 2c). No further selection step is applied to the segments for analysis, resulting in a total number of segments  $K = N_p(N_p - 1)/2 \sim 400 - 600$  per temperature. Notice that such a large number of segments, each being a different sequence, permits measuring many sequences in a single unzipping experiment. In this regard, the unzipping approach is high throughout compared to oligo hybridization experiments, where the measurement of melting curves must be repeated for every oligo sequence.

The entropy of hybridization,  $\Delta S_{0,k}(T)$ , of each segment  $k$  is given by

$$\Delta S_{0,k}(T) = \frac{\partial f_{m,k}(T)}{\partial T} \Delta x_k(f_{m,k}(T), T) + \int_0^{f_{m,k}(T)} \frac{\partial \Delta x_k(f, T)}{\partial T} df, \quad (2)$$

with  $\Delta x_k$  the extension of segment  $k$  (Sec. 3, “Methods”). Equation (2) is analogous to the Clausius-Clapeyron equation<sup>20,35,53</sup> in classical thermodynamics. Here,  $f$  and  $x$  are the equivalent quantities of pressure and volume in hydrostatic systems. The r.h.s. of Eq. (2) depends on the average unzipping force of segment  $k$  measured at different temperatures,  $f_{m,k}(T)$ , according to the equal area Maxwell construction for segment  $k$  (colored horizontal dashed lines in Fig. 2c).  $f_{m,k}(T)$  varies linearly with  $T$ , all segments showing the same slope—0.165(3)pN/K within statistical errors (Fig. 2b and Supplementary Table 3). The integral in Eq. (2) accounts for the work needed to stretch the ssDNA and orient the molecule along the pulling axis between zero force and  $f_{m,k}(T)$  (Supplementary Fig. 6A and Table 3). Equation (2) applied to the full FEC gives the hairpin total entropy of hybridization (Supplementary Fig. 6B).

To apply Eq. (2) for a given segment  $k$ , we must identify the DNA sequence limited by the initial and final peaks. A WLC curve passing through a peak at  $(x, f)$  gives the number  $n$  of unzipped bases at that peak (dashed-grey lines in segment  $\Delta x_k$ ). The initial and final values  $n_A$  and  $n_B$  (orange segment in Fig. 2c) identify the DNA sequence of that segment. Let  $k = 1, 2, \dots, K$  enumerate the different segments. The entropy of segment  $k$  at zero force and temperature  $T$  in the NN model is given by the sum of the individual entropies of all adjacent NNBP within that segment,

$$\Delta S_{0,k}(T) = \sum_{i=AA, CA, \dots} c_{k,i} \Delta S_i(T), \quad (3)$$

where the sum runs over the ten independent NNBP parameters labeled by the index  $i$ , and  $\Delta S_i$  is the entropy of motif  $i$  with multiplicity  $c_{k,i}$ , i.e., the number of times motif  $i$  appears in segment  $k$ . The entropy  $\Delta S_{0,k}(T)$  in the l.h.s of Eq. (3) is measured using Eq. (2), and  $c_{k,i}$  for each motif is obtained from the segment sequence. A stochastic gradient descent algorithm has been designed to solve the system of  $K$  non-homogeneous linear equations in Eq. (3) and derive the  $\Delta S_i$  parameters at each  $T$  (Sec. 4, Methods). The results for the  $T$ -dependent DNA NNBP entropies  $\Delta S_i$  are shown in Fig. 2d and reported in Supplementary Table 4. To determine the statistical errors of  $\Delta S_i(T)$ , we have propagated the values of the elastic parameters at the limits of their confidence interval. Minimum and maximum values for  $\Delta S_i(T)$  set the confidence intervals with the corresponding mean (Supplementary Methods, Sec. 5). The same method has been applied to all NNBP thermodynamic parameters.

### NNBP free energies and enthalpies

From the previously derived NNBP entropies  $\Delta S_i(T)$ , we can also derive the NNBP enthalpies,  $\Delta h_i(T)$ , from the relation,

$$\Delta h_i(T) = \Delta g_i(T) + T \Delta S_i(T), \quad (4)$$

with  $\Delta g_i(T)$  the free energies of the different motifs. The  $\Delta g_i(T)$  values are derived via a Monte Carlo optimization based on the prediction of the theoretical FDC according to the NN model<sup>28,29,40</sup>. The equilibrium FDC is obtained by calculating the equilibrium force at different values of the trap position given a set of energies and elastic parameters. At each step,  $\lambda$  (Eq. (1)) is increased by a fixed  $\Delta\lambda = 3$  nm. The contribution of each element of the molecular construct (optical trap, dsDNA handles, ssDNA, and hairpin diameter) is computed. For a given  $\lambda$  and number of unzipped base pairs  $n$ , the corresponding applied force,  $f$ , is retrieved by inverting Eq. (1). This calculation is repeated for all values of  $n$ . For a given  $\lambda$ , the total energy of the molecular system has two competing contributions: the positive stretching free energy,  $\Delta G_{el}(n, f)$ , acting as an externally applied work to unfold the hairpin, and the negative hybridization free energy,  $\Delta G_0(n)$ , which keeps the hairpin folded. The equilibrium values of  $n^*$  and  $f$  are determined by finding the absolute minimum over  $n$  of  $\Delta G(n, f)$  for that  $\lambda$ . At each

force rip, it is fulfilled that  $\Delta G_{el}(\Delta n^*, f) = \Delta G_0(\Delta n^*)$  rendering the equilibrium FDC a sawtooth pattern made of a sequence of gentle slopes separated by force rips (Supplementary Methods, Sec. 4). The derivation of the equilibrium FDC for each set of energies is the step in an optimization Monte Carlo algorithm used to minimize the error between the theoretical and the experimental FDCs in Fig. 1b (Sec. 5, “Methods”). This procedure gives the eight NNBP independent free energies. The other two parameters (GC/CG and TA/AT) are obtained from the circular symmetry relations<sup>38–40</sup>.

Fits are shown in Fig. 3a for three selected temperatures, and the  $\Delta g_i(T)$  are shown in Fig. 3b (see also Supplementary Table 5). Results (blue circles) agree with the unified oligonucleotide (UO) dataset (black line) and the energy parameters obtained by Huguet et al. in ref. 40 (grey line). In this reference, unzipping experiments at room temperature (298K) were combined with melting temperature data of oligo hybridization over the vastly available literature. Overall agreement is observed, except for some motifs such as AC/TG and GA/CT where the UO energies are lower. The ten NNBP enthalpies were obtained from Eq. (4) at each  $T$  and are shown in Fig. 2d (see also Supplementary Table 6). The agreement between the  $\Delta g_i(T)$  values in Fig. 3b with previous measurements under the assumption  $\Delta c_{p,i} = 0$  for all motifs<sup>40,46</sup>, underlines the strong compensation between the temperature-dependent enthalpies and entropies shown in Fig. 2d that mask the finite  $\Delta c_{p,i}$ 's.

### NNBPs heat capacity changes

The temperature-dependent NNBP entropies and enthalpies permitted us to derive the heat capacity changes  $\Delta c_{p,i}$  for all motifs by using the relations,

$$\Delta S_i = \Delta S_{m,i} + \Delta c_{p,i} \log(T/T_{m,i}) \quad (5a)$$

$$\Delta h_i = \Delta h_{m,i} + \Delta c_{p,i}(T - T_{m,i}), \quad (5b)$$

where  $T_{m,i}$  is the melting temperature of motif  $i$  where  $\Delta g_i(T_{m,i}) = 0$ , and  $\Delta S_{m,i}$  and  $\Delta h_{m,i}$  are the entropy and enthalpy at  $T_{m,i}$ , fulfilling  $\Delta h_{m,i} = T_{m,i} \Delta S_{m,i}$ . To derive the ten  $\Delta c_{p,i}$ , we fit the NNBP entropies to the equation  $A_i + \Delta c_{p,i} \log(T)$ , being  $A_i = \Delta S_{m,i} - \Delta c_{p,i} \log(T_{m,i})$ . The results are shown in Fig. 4a and Table 1 (column 1). From the  $\Delta c_{p,i}$ , we combined Eqs. (5) with Eq. (4) to fit the experimental values of  $\Delta g_i(T)$  (blue dashed lines in Fig. 3b) to obtain  $T_{m,i}$ . From the  $T_{m,i}$ , we retrieve  $\Delta S_{m,i}$  and  $\Delta h_{m,i}$  from Eqs. (5a), (5b) (red and blue dashed lines in Fig. 2d). The fitting procedure is described in Supplementary Methods, Sec. 6. Results for  $T_{m,i}$ ,  $\Delta S_{m,i}$  and  $\Delta h_{m,i}$  are shown in Fig. 4b and Table 1. Notice the high  $T_m$  values of the individual motifs, a consequence of the high enthalpies of the NN motifs.

### Discussion

We measured the free energies, entropies, and enthalpies in the temperature range 7–42 °C at the level of single nearest-neighbor base pairs (NNBP). We have mechanically unzipped a 3.6kbp DNA hairpin using a temperature-jump optical trap. The DNA sequence is long enough to permit us to accurately derive the ten NNBP free-energy parameters,  $\Delta g_i$ , by statistical modeling of the force-distance curve (FDC)<sup>29,40</sup>. At first sight, the  $\Delta g_i$  values (Fig. 3b) vary linearly with temperature due to the compensation of enthalpy and entropy in Eq. (4). This compensation masks the temperature dependence of enthalpies,  $\Delta h_i$ , and entropies,  $\Delta S_i$ , (cf. Eqs. (5)) arising from a finite  $\Delta c_p$ , rendering  $\Delta g_i = \Delta h_i - T \Delta S_i$  linear in  $T$ . We have introduced an approach to derive the  $T$ -dependent entropies by combining the Clausius-Clapeyron relation in force (Eq. (2)) and the nearest-neighbor (NN) model for duplex formation. We implemented a tailored stochastic gradient descent algorithm to extract the ten  $T$ -dependent NNBP entropy parameters,  $\Delta S_i$ . Together with the  $\Delta g_i$  values, the ten enthalpy



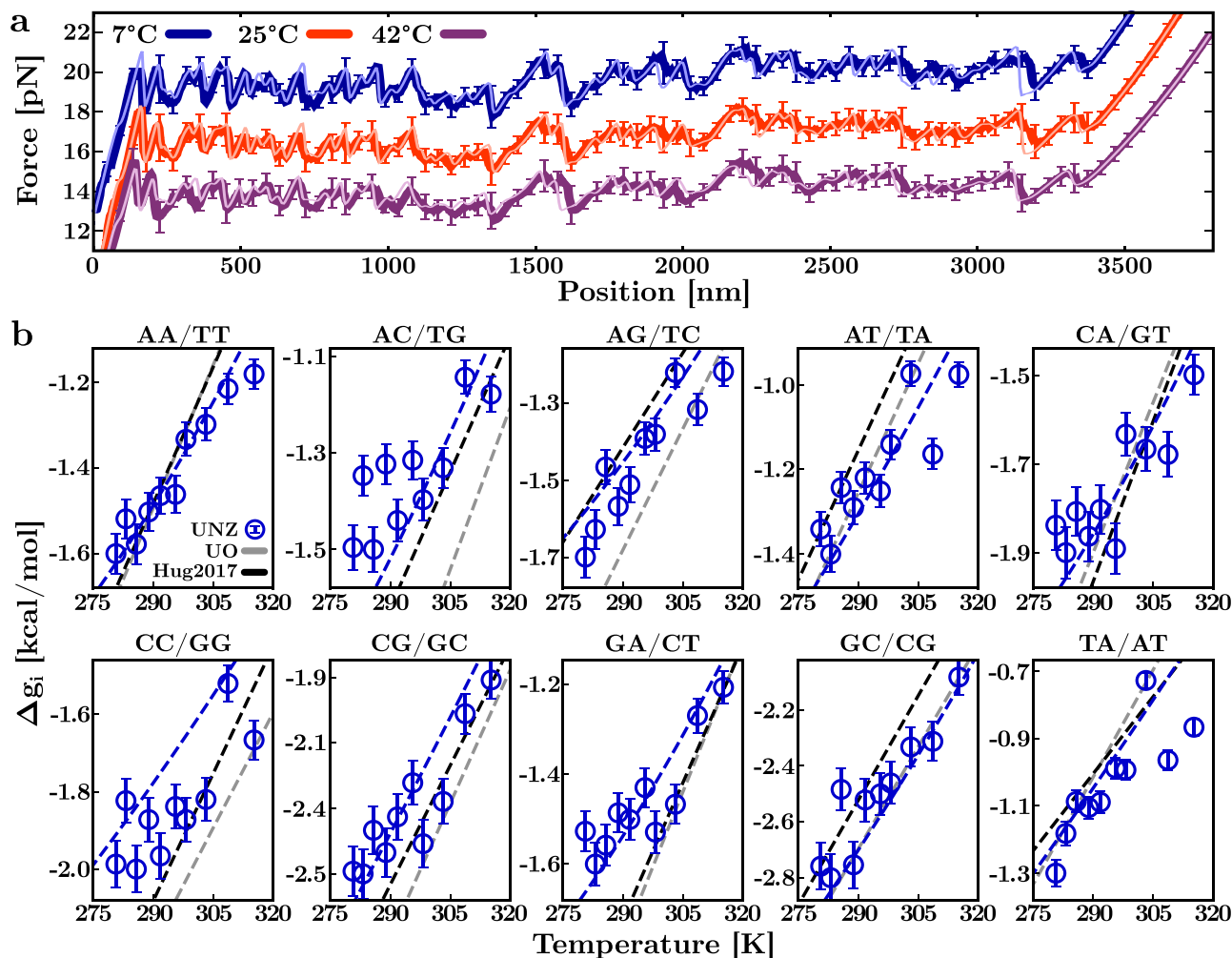


**Fig. 3 | T-dependence of the NNBP DNA free energies.** **a** Experimental FDCs (dark-colored lines) and theoretical predictions (light-colored lines) at 7 °C, 25 °C, and 42 °C. Analogous results have been obtained at all temperatures (Supplementary Fig. 8). **b** Results for the ten NNBP DNA free energies (Supplementary Table 5). The free energy of motifs GC/CG and TA/AT has been computed with circular symmetry

relations. A fit to data (blue line) has been added to compare with predictions by the UO (grey line) and Huguet et al.<sup>40</sup> (black line) sets. All data are presented as mean values  $\pm$  SE (see Supplementary Methods, Sec. 5). Source data are provided as a Source Data file.

parameters,  $\Delta h_i$ , readily follow. Notice that a direct comparison of  $\Delta s_i$  and  $\Delta h_i$  values between our experiments and those in the existing literature can appear misleading. Our  $\Delta s_i$  and  $\Delta h_i$  are temperature dependent, while those in the literature are temperature independent. Which temperature should be chosen to make a comparison? In Supplementary Fig. 9, we chose  $T_m$  as the temperature for the comparison. However, one might also choose the physiological temperature  $T = 37$  °C instead, as several web-server predicting tools do. As we can see from Fig. 3b, an overall agreement is observed between the free energies of the different motifs measured from single-molecule unzipping and bulk experiments despite the differences in the experimental conditions and techniques. The correlation between the NNBP energy values and the sequence motif (GC vs AT content, purine-purine stacking, e.g., GG/CC versus GC/CG) is not straightforward. Despite attempts to find correlation patterns between the NNBP type and structural parameters informative of the relative displacements of base pairs at each base pair step (twist, slide, roll,...)<sup>56</sup>, correlations at the NNBP energy level prove difficult due to the complexity of the stacking interactions within base pairs that are highly sensitive to the interactions between electric charges in the aromatic rings. Fitting the results to Eqs. (5), we have obtained the  $\Delta c_{p,i}$  and  $T_{m,i}$  values for the ten motifs (Fig. 4 and Table 1). Upon averaging over all motifs we get  $\overline{\Delta c_p} = -30(10)$  cal mol<sup>-1</sup>K<sup>-1</sup>bp<sup>-1</sup>. This must be compared to the highly

dispersed results from bulk experiments ranging between  $-20$  and  $-160$  cal mol<sup>-1</sup>K<sup>-1</sup>bp<sup>-1</sup>, depending on the experimental technique, setup, and DNA sequence<sup>2,15</sup>. In contrast, recent molecular dynamic simulations estimated an average  $\Delta c_p \sim -30$  cal mol<sup>-1</sup>K<sup>-1</sup>bp<sup>-1</sup><sup>157,58</sup>, in agreement with our results.

Force spectroscopy emerges as a reliable approach to accurately derive the energy parameters in NAs. Unzipping experiments control the unfolding reaction by moving the force-sensing device (e.g., optical trap in optical tweezers and cantilever in AFM). In DNA hairpins of a few kb, the sequence contains all ten NN motifs repeated several times, ensuring their reliable statistical sampling in single-DNA unzipping experiments. The high-temporal resolution combined with the sub-kcal/mol accuracy of work measurements permits us to derive the ten NN energy parameters at different temperatures. The main requirement of unzipping experiments is an accurate model of the elastic response of the single-stranded DNA (ssDNA). We have fit the last part of the unzipping FDCs to the worm-like chain model, known to fit data well at high-salt conditions (1M NaCl) where ssDNA excluded-volume effects are negligible<sup>54</sup>. Salt concentration might also affect the  $\Delta c_{p,i}$  values. As these are related to the change in configurational entropy upon duplex formation, salt-dependent  $\Delta c_p$ 's might indicate a change in conformational heterogeneity in either the dissociated or hybridized strands upon varying salt. We notice that the method presented

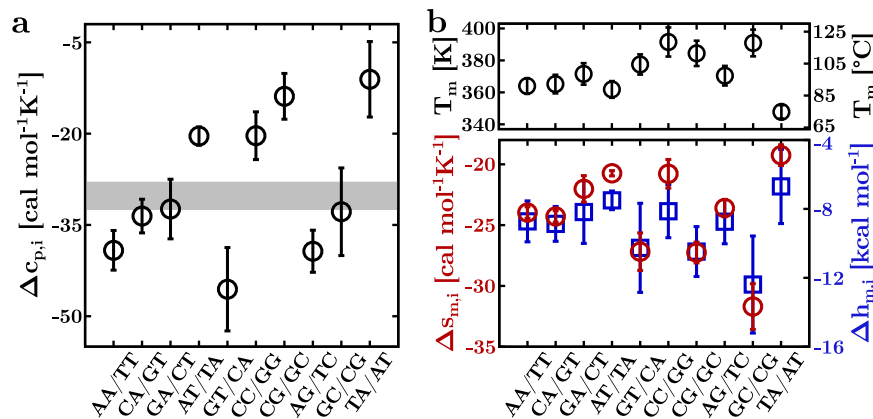


**Fig. 4 | The DNA NNBP thermodynamics.** **a** Measured heat capacity change per motif. The grey band shows the range of  $\Delta c_p$  values per motif reported in ref. 15. **b** Melting temperatures (top), entropies, and enthalpies at  $T_m$  (bottom) for each of

the ten NNBP parameters. Results for motifs GC/CG and TA/AT have been derived by applying circular symmetry relations. All data are presented as mean values  $\pm$  SE. Source data are provided as a Source Data file.

**Table 1 | Measured heat capacity change ( $\Delta c_{p,i}$ ), entropy ( $\Delta s_{m,i}$ ), enthalpy ( $\Delta h_{m,i}$ ), and melting temperature ( $T_{m,i}$ ) for the ten NNBP motifs**

NNBP	$\Delta c_{p,i}$ [cal mol <sup>-1</sup> K <sup>-1</sup> ]	$\Delta s_{m,i}$ [cal mol <sup>-1</sup> K <sup>-1</sup> ]	$\Delta h_{m,i}$ [kcal mol <sup>-1</sup> ]	$T_{m,i}$ [K]
AA/TT	-39(3)	-24.0(5)	-8.7(9)	364(5)
AC/TG	-34(3)	-24.3(5)	-9(1)	365(6)
AG/TC	-32(5)	-22(1)	-8(2)	371(7)
AT/TA	-20(1)	-20.7(2)	-7.5(5)	362(5)
CA/GT	-46(7)	-27(1)	-10(3)	377(6)
CC/GG	-20(4)	-21(1)	-8(1)	391(9)
CG/GC	-14(4)	-27.2(8)	-10(1)	384(8)
GA/CT	-39(3)	-23.6(7)	-9(1)	370(6)
GC/CG	-33(7)	-32(2)	-12(3)	391(8)
TA/AT	-11(6)	-19.2(8)	-7(2)	348(4)

Motifs GC/CG and TA/AT have been derived by applying the circular symmetry relations. All data are presented as mean values  $\pm$  SE (reported in brackets).

in this work is general and can be straightforwardly extended to other experimental conditions (e.g., different salt concentrations or ionic strength).

How do our results compare to those derived from calorimetric melting experiments? The structure of the unfolded state differs in unzipping and thermal denaturation experiments, a fully stretched ssDNA at a given force, and a random coil at zero force, respectively. Their free energy difference equals the work to stretch the ssDNA from the random coil to the stretched conformation. Moreover, hybridization and unzipping differ in the order of the unfolding reactions: while hybridization of two complementary oligos,  $A$  and  $\bar{A}$ , is a bimolecular reaction  $A + \bar{A} \rightleftharpoons AA$ , hairpin unzipping is a unimolecular reaction  $A \rightleftharpoons B$  between the folded and unfolded conformations. Such difference is apparent in the dependence of  $T_m$  on the enthalpy  $\Delta H_0^m$  and entropy  $\Delta S_0^m$  of folding. For a bimolecular reaction, the value of  $T_m$  explicitly depends on the total oligo concentration  $c$ , with  $\Delta S_0^m, \Delta H_0^m$  taken at the reference 1M salt condition (Eq. (10), “Methods”). Instead, for the unimolecular unzipping reaction,  $T_m = \Delta H_0^m / \Delta S_0^m$  does not include the entropy of mixing the dissociated strands. We expect that temperature-dependent enthalpies  $\Delta h_i$  are equal for hybridization and unzipping, whereas entropies  $\Delta s_i$  should differ due to the entropy of mixing. We have determined the homogeneous entropy correction  $\delta \Delta s$  to the total entropy  $\Delta S_0^m$  between hybridization (bimolecular) and unzipping (unimolecular) reactions (Sec. 6, Methods). The correction

is an intensive quantity that is independent of oligo sequence and length,  $\delta \Delta s = 6(1) \text{ cal mol}^{-1} \text{K}^{-1} \sim 4R \log 2$ , where  $R = 1.987 \text{ cal mol}^{-1} \text{K}^{-1}$  is the ideal gas constant (Eq. (11), “Methods”). This value has been obtained by comparing the  $T_m$  values predicted by our energy parameters using Eq. (10) with the experimental values obtained for DNA duplexes in ref. 59 at 1020 mM NaCl and  $c = 2 \mu\text{M}$ . The results of such a comparison are shown in Supplementary Fig. 10. Practically, the effect of the entropic correction  $\delta \Delta s$  on  $T_m$  is small as it is  $\sim 3 - 4$  times lower than the average NNBP’s entropy  $\Delta s_m \sim -20 \text{ cal mol}^{-1} \text{K}^{-1}$  (cf. Table 1). Notice that  $\Delta S_0^m$  is extensive, growing linearly with the oligo length, whereas  $\delta \Delta s$  is intensive. Therefore, the correction  $\delta \Delta s \sim 5 \text{ cal mol}^{-1} \text{K}^{-1}$  is negligible for sufficiently large oligos, being already 5% for oligos of just ten nucleotides and further decreasing for longer DNAs (see Supplementary Table 7).

The remarkable accuracy of the nearest-neighbor model for reproducing the experimentally measured force-distance curves permitted us to derive the temperature-dependent DNA energy parameters. One might ask whether there are deviations from the NN model, e.g., in the form of next-to-nearest neighbor (NNN) effects predicted to be important for some tetranucleotide motifs<sup>60</sup>. However, NNN effects might be difficult to observe in unzipping experiments of long DNA hairpins. Our method averages local effects over the whole sequence hiding potential deviations from the NN model at some locations. Unzipping studies on suitably designed short DNA hairpins containing specific NNN motifs would be more appropriate to address this problem. In this case, determining the elastic response of the specific ssDNA sequence would also be necessary<sup>61</sup>. The unzipping method might also be applicable to derive the temperature-dependent energy parameters of RNA, where finite  $\Delta c_p$  effects are particularly relevant to the RNA folding problem. Previous studies at room temperature show that RNA unzipping is an irreversible process driven by stem-loops forming along the unpaired strands that compete with the hybridization of the native stem<sup>47</sup>. Such irreversible and kinetic effects suggest higher  $\Delta c_{p,i}$  values in RNA compared to DNA. DNA thermodynamics down to 0 °C might find applications for predicting DNA thermodynamics at low temperatures and cold denaturation effects. Estimates based on our  $\Delta c_{p,i}$  values show that the most stable DNA hairpins ending a tetraloop predict cold denaturation temperatures lower than  $\sim -90 \text{ °C}$  (Supplementary Fig. 11), raising questions about the importance of cold denaturation effects for cryophile organisms surviving in extremely cold environments<sup>62</sup>. Finally, our results have implications for determining the DNA force fields used in molecular dynamics simulations of DNA conformational kinetics<sup>63</sup>, essential for computational studies of NAs in general.

## Methods

### Molecular construct and experimental setup

We used a temperature-jump optical trap<sup>20</sup> (OT) to unzip a 3593bp DNA hairpin flanked by short (29bp) DNA handles and ending with a GAAA tetraloop. Experiments have been carried out in the temperature range [7,42] °C in a buffer of 1M NaCl, 10 mM Tris-HCl (pH 7.5), and 1 mM EDTA. Experiments have been performed at a constant pulling speed,  $v = 100$  nm/s. We sampled 5–6 different molecules at each temperature, collecting a minimum of ~50 unfolding-folding trajectories per molecule. To change the temperature inside the microfluidics chamber, the MiniTweezers setup implements a heating laser of wavelength  $\lambda = 1435$  nm. This device allows for increasing the temperature by discrete amounts of  $\Delta T \sim +2.5$  °C up to a maximum of  $\sim +30$  °C with respect to the environment temperature,  $T_0$ . To carry out experiments at low temperatures, the OT is placed into an insulated box integrated with a refrigeration system (ice-box) and containing a water reservoir. The ice-box is cooled down to subzero temperatures in order for the water to freeze. After the refrigeration is turned off, the temperature stabilizes at 5 °C. This device allowed to carry out experiments at a minimum temperature of 7 °C. The design of the microfluidics chamber has been chosen to damp convection effects caused by the laser non-uniform temperature, which may produce a hydrodynamics flow between medium regions (water) at different  $T$ .

The temperature inside the microfluidic chamber is measured from the viscosity,  $\eta$ , of the buffer solution in the proximity of the micropipette, i.e., the region where experiments are carried out. To measure  $\eta$ , we use Stokes' law for the force exerted on a sphere of radius  $R$  dragged at speed  $v$  in a viscous fluid,  $f = -6\pi\eta Rv$ . This is done by trapping an anti-digoxigenin (AD) bead with the optical tweezers and moving the fluidics chamber between two fixed positions along one direction (Ex., the  $x$ -axis). The  $T$ -dependence of  $\eta$  follows the well-known Vogel-Fulcher-Tammann-Hesse equation  $\eta = \eta_0 e^{B/(T-T_0)}$ , where  $\eta_0$ ,  $B$ , and  $T_0$  are empirical fitting parameters as explained in ref. 20. Inverting this equation gives the temperature  $T$  inside the chamber from the experimentally measured viscosity. This procedure is done upon incrementing the laser power output from zero to maximum and is repeated many times during the experiments to ensure the correct measurement of the temperature. Finally, convection effects were minimized using Kohler's illumination combined with a suitable design of the microfluidics chamber to reduce heat absorption. A full description of the temperature-jump optical trap instrument can be found in ref. 20.

In a typical optical tweezers (OT) unzipping experiment<sup>64</sup>, a molecule is tethered between two polystyrene beads through specific interactions at its ends. One end of the molecule is labeled with a digoxigenin (DIG) tail, which binds to a 3  $\mu$ m diameter polystyrene bead coated with anti-DIG (AD). The other end is labeled with biotin (BIO), which binds to a 2  $\mu$ m diameter streptavidin-coated bead (SA). The AD bead is optically trapped, while the SA bead is immobilized by air suction at the tip of a glass micropipette. During a pulling cycle, the optical trap moves between two fixed positions. At the beginning of the unzipping protocol, the molecule is folded. Upon increasing the distance between the trap and the pipette ( $\lambda$ ), an external force is applied to the molecular ends. This causes the hairpin to progressively unzip in a stick-slip process characterized by a sequence of slopes and force rips (FDC sawtooth pattern). Each rip corresponds to the cooperative unfolding of a group of bp due to the applied (external) work exceeding the hybridization (internal) energy. When the molecule is totally unzipped, the rezipping protocol starts;  $\lambda$  is decreased, and the molecule folds back reversibly to the hairpin (native) state. We notice that the number of bp released in each unfolding event depends on the sequence composition, making the FDC the DNA footprint.

### ssDNA elastic model

The total hairpin extension with  $n$  unzipped bases at force  $f$  and temperature  $T$ ,  $x(n, f, T)$ , is given by the sum of the ssDNA extension

( $x_{ss}(f, n, T)$ ) plus the contribution of the double helix diameter ( $x_d(f, T)$ ). The ssDNA elastic response has been modeled according to the Worm-Like chain (WLC), which reads

$$f(x, n, T) = \frac{k_B T}{4l_p} \left[ \left( 1 - \frac{x}{nd_b} \right)^{-2} - 1 + 4 \frac{x}{nd_b} \right], \quad (6)$$

where  $k_B$  is the Boltzmann constant, and  $T$  is the temperature,  $l_p$  is the persistence length,  $d_b$  is the interphosphate distance and  $n$  is the number of ssDNA bases. Notice that the computation of the ssDNA extension requires inverting Eq. (6)<sup>51</sup>.

The observed increase in the ssDNA extension with  $T$  at a given force (Fig. 1b) demonstrates that  $l_p$  and  $d_b$  are  $T$ -dependent. This contrasts with the original assumption in the WLC model that  $l_p$  and  $d_b$  are temperature independent and  $x_{ss}$  decreasing with  $T$  at a given force. Remarkably, Eq. (6) accurately describes our data as stacking effects in mixed purine-pyrimidine sequences are negligible in our experimental conditions<sup>54</sup>.

The contribution of the hairpin diameter to  $x$  is given by the projection of the helix diameter in the direction of propagation of the force. It is described as a free dipole in an external force field and is modeled by the FJC model, which reads

$$x_d(f, T) = d \left[ \coth \left( \frac{fd}{k_B T} \right) - \frac{k_B T}{fd} \right], \quad (7)$$

where  $d = 2$  nm is the hairpin diameter<sup>52</sup>.

### The Clausius–Clapeyron equation

In the unzipping experiment, the total trap-pipette distance is given by  $\lambda = x + x_b + 2x_h$ , where  $x$  is the extension of the ssDNA plus the molecular diameter, while  $x_b$  and  $2x_h$  are the bead displacement relative to the trap's center and the extension of the handle, respectively. Starting with the hairpin totally folded, unzipping consists of converting the double-stranded DNA into ssDNA until it is completely unfolded. The free energy needed to fold back the ssDNA into the hairpin and decrease the applied force to zero is given by

$$\Delta G_0(T) = - \int_0^{f_m(T)} \Delta \lambda(f, T) df, \quad (8)$$

where  $\Delta \lambda$  is the total extension change of the hairpin between the initial and final states of the unzipping integrated between zero and the mean unzipping force,  $f_m$ . The comparably high stiffness of the optically trapped bead and the short extension and large persistence length of the dsDNA handles, as compared to the released ssDNA ( $l_p^{ds} = 12.5$  nm and  $l_p^{ss} = 0.77$  nm at 25 °C), permit us to approximate the contributions  $x_b$  and  $2x_h$  to  $\lambda$  as constant near the average unzipping force. Therefore,  $\Delta \lambda \approx \Delta x$ , i.e., equals the ssDNA's extension change only.

The folding entropy can be directly derived from the thermodynamic relation  $\Delta S_0(T) = -\partial \Delta G_0(T)/\partial T$ , which gives

$$\Delta S_0(T) = \frac{\partial f_m(T)}{\partial T} \Delta x(f_m(T), T) + \int_0^{f_m(T)} \frac{\partial \Delta x(f, T)}{\partial T} df. \quad (9)$$

The first term of Eq. (9) is analogous to the Clausius–Clapeyron equation for first-order phase transitions, where  $f$  and  $x$  are equivalent to pressure and volume. The integral term in Eq. (9) accounts for the (positive) entropic contribution to stretch the ssDNA and orient the molecular diameter along the pulling axis from zero to force  $f_m$ .

### Stochastic gradient descent method

The derivation of the DNA NNBP entropies corresponds to solving the non-homogeneous linear system of  $K$  equations and  $l = 8$  parameters

given by Eq. (3). To do this, we used a custom-designed stochastic gradient descent (SGD) algorithm. The model is described in Supplementary Methods, Sec. 3. The application of an optimization algorithm to this problem is made possible by the large data set built accounting for all possible peaks combination, which gives  $K \sim 400\text{--}600 \gg I$  for each experimental  $T$ .

### Derivation of the NNBP free-energies

Starting with an initial guess of the ten independent  $\Delta g_i$ , a random increment of the energies is proposed at each optimization step, and a prediction of the FDC is generated. The latter is given by the competition of two energy contributions at each position of the optical trap ( $x_{\text{tot}}$ ): the energy of the stretched molecular construct acting to unfold the molecule ( $\Delta G_{\text{el}}(x_{\text{tot}})$ ), and the energy of the hybridized bps keeping the hairpin folded ( $\Delta G_0(x_{\text{tot}}, n)$ ). At a given  $x_{\text{tot}}$  and  $n_1$  hybridized bp (Fig. 2a), the hairpin unfolds when  $\Delta G_{\text{el}}(x_{\text{tot}}) > \Delta G_0(x_{\text{tot}}, n_1)$  (force rip) and  $\Delta n = n_2 - n_1$  bp are released lowering the stretching contribution so that  $\Delta G_{\text{el}}(x_{\text{tot}}) < \Delta G_0(x_{\text{tot}}, n_2)$  (see Supplementary Methods, Sec. 4). The error in approximating the experimental FDC with the theoretical one,  $E = (f_{\text{exp}} - f_{\text{theo}})^2$ , drives a Metropolis algorithm: a change of the energy parameters is accepted if the error difference to the previous step is negative ( $\Delta E < 0$ ). Otherwise ( $\Delta E > 0$ ), the proposal is accepted if  $\exp(-\Delta E/T) < r$  with  $r$  a random number uniformly distributed  $r \in U(0, 1)$ . The algorithm continues until convergence (until  $\Delta E$  is smaller than a given threshold) or until the maximum number of iterations is reached. The parameters corresponding to the smallest value of  $E$  are the optimal NNBP free energies.

### Prediction of the oligos melting temperature

The melting temperature for non-self-complementary sequences in bimolecular reactions (hybridization) is given by

$$T_m^{\text{Bi}} = \frac{\Delta H_0^m}{\Delta S_0^m + R \log(c/4)}, \quad (10)$$

where  $\Delta H_0^m = \sum_i \Delta h_i$  ( $\Delta S_0^m = \sum_i \Delta s_i$ ) is the total duplex enthalpy (entropy) at  $T = T_m$ ,  $R = 0.001987 \text{ kcal mol}^{-1} \text{ K}^{-1}$  is the ideal gas constant,  $c$  is the experimental oligo concentration. In contrast, for unimolecular reactions (folding), we found

$$T_m^{\text{Uni}} = \frac{\Delta H_0^m}{\Delta S_0^m + R \log(c/4) + \delta \Delta s}, \quad (11)$$

where  $\delta \Delta s = 4R \log 2$  is a correction to the total entropy  $\Delta S_0^m$ . By subtracting the inverse of Eq. (10) and Eq. (11), one gets

$$\delta \Delta s = \Delta H_0^m \left( \frac{1}{T_m^{\text{Bi}}} - \frac{1}{T_m^{\text{Uni}}} \right), \quad (12)$$

where the term in parenthesis is computed by subtracting the  $T_m$  values predicted by our energy parameters using Eq. (10) to the experimental dataset measured by Ocwzarzy et al. at 1020 mM NaCl and  $c = 2 \mu\text{M}^{39}$  (Supplementary Fig. 10 and Table 7). Finally,  $\Delta H_0^m$  is determined by using our NNBP enthalpy parameters.

### Reporting summary

Further information on research design is available in the Nature Portfolio Reporting Summary linked to this article.

### Data availability

The authors declare that the data supporting the findings of this study are available within the paper, its supplementary information files, the main text, and Supplementary Information. The unzipping data generated in this study have been deposited in the figshare database under

accession code [<https://doi.org/10.6084/m9.figshare.28211567>]. Source data are provided with this paper.

### Code availability

The code developed to analyze the experimental data and derive the DNA thermodynamic parameters of the nearest-neighbor model is available on Code Ocean [<https://codeocean.com/capsule/1145286/tree/v3>].

### References

- Jinek, M. et al. A programmable dual-RNA-guided DNA endonuclease in adaptive bacterial immunity. *Science* **337**, 816–821 (2012).
- Cong, L. et al. Multiplex genome engineering using CRISPR/CAS systems. *Science* **339**, 819–823 (2013).
- Ivanov, I. E. et al. Cas9 interrogates DNA in discrete steps modulated by mismatches and supercoiling. *Proc. Natl Acad. Sci.* **117**, 5853–5860 (2020).
- Rothmund, P. W. Folding DNA to create nanoscale shapes and patterns. *Nature* **440**, 297–302 (2006).
- Douglas, S. M. et al. Self-assembly of dna into nanoscale three-dimensional shapes. *Nature* **459**, 414–418 (2009).
- Castro, C. E. et al. A primer to scaffolded DNA origami. *Nat. Methods* **8**, 221 (2011).
- Chalikian, T. V., Völker, J., Plum, G. E. & Breslauer, K. J. A more unified picture for the thermodynamics of nucleic acid duplex melting: a characterization by calorimetric and volumetric techniques. *Proc. Natl Acad. Sci. USA* **96**, 7853–7858 (1999).
- Vologodskii, A. & Frank-Kamenetskii, M. D. Dna melting and energetics of the double helix. *Phys. Life Rev.* **25**, 1–21 (2018).
- Whitley, K. D., Comstock, M. J. & Chemla, Y. R. Elasticity of the transition state for oligonucleotide hybridization. *Nucl. Acids Res.* **45**, 547–555 (2017).
- Breslauer, K. J., Frank, R., Blöcker, H. & Marky, L. A. Predicting DNA duplex stability from the base sequence. *Proc. Natl Acad. Sci. USA* **83**, 3746–3750 (1986).
- Breslauer, K. J. The shaping of a molecular linguist: How a career studying DNA energetics revealed the language of molecular communication. *J. Biol. Chem.* **296**, 100522 (2021).
- Rouzina, I. & Bloomfield, V. A. Heat capacity effects on the melting of DNA. 1. General aspects. *Biophys. J.* **77**, 3242–3251 (1999).
- Rouzina, I. & Bloomfield, V. A. Heat capacity effects on the melting of DNA. 2. Analysis of nearest-neighbor base pair effects. *Biophys. J.* **77**, 3252–3255 (1999).
- Wu, P., Nakano, S.-i & Sugimoto, N. Temperature dependence of thermodynamic properties for DNA/DNA and RNA/DNA duplex formation. *Eur. J. Biochem.* **269**, 2821–2830 (2002).
- Mikulecky, P. J. & Feig, A. L. Heat capacity changes associated with nucleic acid folding. *Biopolymers* **82**, 38–58 (2006).
- Mikulecky, P. J. & Feig, A. L. Heat capacity changes associated with DNA duplex formation: salt- and sequence-dependent effects. *Biochemistry* **45**, 604–616 (2006).
- Dragan, A., Privalov, P. & Crane-Robinson, C. Thermodynamics of DNA: heat capacity changes on duplex unfolding. *Eur. Biophys. J.* **48**, 773–779 (2019).
- Völker, J., Plum, G. E. & Breslauer, K. J. Heat capacity changes ( $\delta c_p$ ) for interconversions between differentially-ordered DNA states within physiological temperature domains: Implications for biological regulatory switches. *J. Phys. Chem. B* **124**, 5614–5625 (2020).
- Williams, M. C., Wenner, J. R., Rouzina, I. & Bloomfield, V. A. Entropy and heat capacity of DNA melting from temperature dependence of single molecule stretching. *Biophys. J.* **80**, 1932–1939 (2001).
- De Lorenzo, S., Ribezzi-Crivellari, M., Arias-Gonzalez, J. R., Smith, S. B. & Ritort, F. A temperature-jump optical trap for single-molecule manipulation. *Biophys. J.* **108**, 2854–2864 (2015).



21. Nicholson, D. A., Jia, B. & Nesbitt, D. J. Measuring excess heat capacities of deoxyribonucleic acid (DNA) folding at the single-molecule level. *J. Phys. Chem. B* **125**, 9719–9726 (2021).
22. Rief, M., Clausen-Schaumann, H. & Gaub, H. E. Sequence-dependent mechanical mechanics of single DNA molecules. *Nat. Struct. Biol.* **6**, 346–349 (1999).
23. Krautbauer, R., Rief, M. & Gaub, H. E. Unzipping DNA oligomers. *Nano Lett.* **3**, 493–496 (2003).
24. Bacic, L., Sabantsev, A. & Deindl, S. Recent advances in single-molecule fluorescence microscopy render structural biology dynamic. *Curr. Opin. Struct. Biol.* **65**, 61–68 (2020).
25. Bustamante, C., Bryant, Z. & Smith, S. B. Ten years of tension: single-molecule DNA mechanics. *Nature* **421**, 423–427 (2003).
26. Moffitt, J. R., Chemla, Y. R., Smith, S. B. & Bustamante, C. Recent advances in optical tweezers. *Annu. Rev. Biochem.* **77**, 205–228 (2008).
27. Roy, R., Hohng, S. & Ha, T. A practical guide to single-molecule fret. *Nat. Methods* **5**, 507–516 (2008).
28. Huguet, J. M., Forns, N. & Ritort, F. Statistical properties of metastable intermediates in DNA unzipping. *Phys. Rev. Lett.* **103**, 248106 (2009).
29. Huguet, J. M. et al. Single-molecule derivation of salt dependent base-pair free energies in DNA. *Proc. Natl Acad. Sci. USA* **107**, 15431–15436 (2010).
30. Koch, S. J., Shundrovsky, A., Jantzen, B. C. & Wang, M. D. Probing protein-DNA interactions by unzipping a single DNA double helix. *Biophys. J.* **83**, 1098–1105 (2002).
31. Rudnizky, S. et al. Single-molecule dna unzipping reveals asymmetric modulation of a transcription factor by its binding site sequence and context. *Nucleic Acids Res.* **46**, 1513–1524 (2018).
32. Khamis, H., Rudnizky, S., Melamed, P. & Kaplan, A. Single molecule characterization of the binding kinetics of a transcription factor and its modulation by DNA sequence and methylation. *Nucleic Acids Res.* **49**, 10975–10987 (2021).
33. Camunas-Soler, J. et al. Single-molecule kinetics and footprinting of DNA bis-intercalation: the paradigmatic case of thiocoraline. *Nucl. Acids Res.* **43**, 2767–2779 (2015).
34. Shrestha, P. et al. Single-molecule mechanical fingerprinting with DNA nanoswitch calipers. *Nat. Nanotechnol.* **16**, 1362–1370 (2021).
35. Rico-Pasto, M., Zaltron, A., Davis, S. J., Frutos, S. & Ritort, F. Molten globule-like transition state of protein barnase measured with calorimetric force spectroscopy. *Proc. Natl Acad. Sci. USA* **119**, 2112382119 (2022).
36. DeVoe, H. & Tinoco Jr, I. The stability of helical polynucleotides: base contributions. *J. Mol. Biol.* **4**, 500–517 (1962).
37. Crothers, D. M. & Zimm, B. H. Theory of the melting transition of synthetic polynucleotides: evaluation of the stacking free energy. *J. Mol. Biol.* **9**, 1–9 (1964).
38. Gray, D. M. & Tinoco Jr, I. A new approach to the study of sequence-dependent properties of polynucleotides. *Biopolymers* **9**, 223–244 (1970).
39. Licinio, P. & Guerra, J. C. O. Irreducible representation for nucleotide sequence physical properties and self-consistency of nearest-neighbor dimer sets. *Biophys. J.* **92**, 2000–2006 (2007).
40. Huguet, J. M., Ribezzi-Crivellari, M., Bizarro, C. V. & Ritort, F. Derivation of nearest-neighbor DNA parameters in magnesium from single molecule experiments. *Nucleic Acids Res.* **45**, 12921–12931 (2017).
41. Gotoh, O. & Tagashira, Y. Stabilities of nearest-neighbor doublets in double-helical DNA determined by fitting calculated melting profiles to observed profiles. *Biopolymers* **20**, 1033–1042 (1981).
42. Delcourt, S. G. & Blake, R. Stacking energies in DNA. *J. Biol. Chem.* **266**, 15160–15169 (1991).
43. Doktycz, M. J., Goldstein, R. F., Paner, T. M., Gallo, F. J. & Benight, A. S. Studies of DNA dumbbells. I. Melting curves of 17 DNA dumbbells with different duplex stem sequences linked by t4 endloops: evaluation of the nearest-neighbor stacking interactions in DNA. *Biopolymers* **32**, 849–864 (1992).
44. SantaLucia, J., Allawi, H. T. & Seneviratne, P. A. Improved nearest-neighbor parameters for predicting DNA duplex stability. *Biochem* **35**, 3555–3562 (1996).
45. Sugimoto, N., Nakano, S.-i., Yoneyama, M. & Honda, K.-i. Improved thermodynamic parameters and helix initiation factor to predict stability of DNA duplexes. *Nucleic Acids Res.* **24**, 4501–4505 (1996).
46. SantaLucia, J. A unified view of polymer, dumbbell, and oligonucleotide DNA nearest-neighbor thermodynamics. *Proc. Natl Acad. Sci. USA* **95**, 1460–1465 (1998).
47. Rissone, P., Bizarro, C. V., Ritort, F. Stem-loop formation drives RNA folding in mechanical unzipping experiments. *Proc. Natl. Acad. Sci. USA* **119**, e2025575119 (2022).
48. Zuker, M. Mfold web server for nucleic acid folding and hybridization prediction. *Nucleic Acids Res.* **31**, 3406–3415 (2003).
49. Lorenz, R. et al. Vienna RNA package 2.0. *Algorithms Mol. Biol.* **6**, 1–14 (2011).
50. Dwight, Z., Palais, R. & Wittwer, C. T. umelt: prediction of high-resolution melting curves and dynamic melting profiles of PCR products in a rich web application. *Bioinform* **27**, 1019–1020 (2011).
51. Severino, A., Monge, A. M., Rissone, P. & Ritort, F. Efficient methods for determining folding free energies in single-molecule pulling experiments. *J. Stat. Mech. Theory Exp.* **2019**, 124001 (2019).
52. Woodside, M. T. et al. Direct measurement of the full, sequence-dependent folding landscape of a nucleic acid. *Science* **314**, 1001–1004 (2006).
53. Smith, S. B., Cui, Y. & Bustamante, C. Overstretching B-DNA: the elastic response of individual double-stranded and single-stranded DNA molecules. *Science* **271**, 795–799 (1996).
54. Viader-Godoy, X., Pulido, C., Ibarra, B., Manosas, M. & Ritort, F. Cooperativity-dependent folding of single-stranded DNA. *Phys. Rev. X* **11**, 031037 (2021).
55. Rico-Pasto, M. & Ritort, F. Temperature-dependent elastic properties of DNA. *Biophys. Rep.* **2**, 100067 (2022).
56. Calladine, C. R. & Drew, H. Understanding DNA: the Molecule and How It Works. (Academic Press, 1997).
57. Lomzov, A. A., Vorobjev, Y. N. & Pyshnyi, D. V. Evaluation of the Gibbs free energy changes and melting temperatures of DNA/DNA duplexes using hybridization enthalpy calculated by molecular dynamics simulation. *J. Phys. Chem. B* **119**, 15221–15234 (2015).
58. Hadži, S. & Lah, J. Origin of heat capacity increment in DNA folding: the hydration effect. *Biochim. Biophys. Acta Gen. Subj.* **1865**, 129774 (2021).
59. Owczarzy, R., Moreira, B. G., You, Y., Behlke, M. A. & Walder, J. A. Predicting stability of DNA duplexes in solutions containing magnesium and monovalent cations. *Biochemistry* **47**, 5336–5353 (2008).
60. Balaceanu, A. et al. Modulation of the helical properties of DNA: next-to-nearest neighbour effects and beyond. *Nucleic Acids Res.* **47**, 4418–4430 (2019).
61. Alemany, A. & Ritort, F. Determination of the elastic properties of short ssDNA molecules by mechanically folding and unfolding DNA hairpins. *Biopolymers* **101**, 1193–1199 (2014).
62. D’Amico, S. et al. Psychrophilic microorganisms: challenges for life. *EMBO Rep.* **7**, 385–389 (2006).
63. Liao, Q. et al. Long time-scale atomistic simulations of the structure and dynamics of transcription factor-DNA recognition. *J. Phys. Chem. B* **123**, 3576–3590 (2019).
64. Rissone, P., Severino, A., Pastor, I. & Ritort, F. Universal cold RNA phase transitions. *Proc. Natl Acad. Sci. USA* **121**, 2408313121 (2024).

## Acknowledgements

P.R. was supported by the Angelo Della Riccia Foundation. M.R.-P. was supported by the Spanish Research Council JDC2022-049996-I. F.R. was supported by Spanish Research Council Grant PID2019-111148GB-I00 and the Institució Catalana de Recerca i Estudis Avançats (F.R., Academia Prize 2018).

## Author contributions

P.R. and M.R.-P. carried out the experiments. S.B.S. designed and built the instrument. P.R. and M.R.-P. analyzed the data. P.R., M.R.-P., and F.R. designed the research. P.R. and F.R. wrote the paper.

## Competing interests

The authors declare the following financial competing interests: Steven B. Smith makes and sells the optical tweezers that have been used for this work. All other co-authors declare no competing interests.

## Additional information

**Supplementary information** The online version contains supplementary material available at <https://doi.org/10.1038/s41467-025-57340-5>.

**Correspondence** and requests for materials should be addressed to F. Ritort.

**Peer review information** *Nature Communications* thanks Beatrice Soh and the other, anonymous, reviewer(s) for their contribution to the peer review of this work. A peer review file is available.

**Reprints and permissions information** is available at <http://www.nature.com/reprints>

**Publisher's note** Springer Nature remains neutral with regard to jurisdictional claims in published maps and institutional affiliations.

**Open Access** This article is licensed under a Creative Commons Attribution-NonCommercial-NoDerivatives 4.0 International License, which permits any non-commercial use, sharing, distribution and reproduction in any medium or format, as long as you give appropriate credit to the original author(s) and the source, provide a link to the Creative Commons licence, and indicate if you modified the licensed material. You do not have permission under this licence to share adapted material derived from this article or parts of it. The images or other third party material in this article are included in the article's Creative Commons licence, unless indicated otherwise in a credit line to the material. If material is not included in the article's Creative Commons licence and your intended use is not permitted by statutory regulation or exceeds the permitted use, you will need to obtain permission directly from the copyright holder. To view a copy of this licence, visit <http://creativecommons.org/licenses/by-nc-nd/4.0/>.

© The Author(s) 2025